

RESEARCH ARTICLE | SEPTEMBER 08 2023

Real-time time-dependent self-consistent field methods with dynamic magnetic fields

Meilani Wibowo-Teale  ; Benjamin J. Ennifer ; Andrew M. Wibowo-Teale 



J. Chem. Phys. 159, 104102 (2023)

<https://doi.org/10.1063/5.0160317>



View
Online



Export
Citation

CrossMark



APL Quantum
Bridging fundamental quantum research with technological applications

Now Open for Submissions
No Article Processing Charges (APCs) through 2024

Submit Today



Real-time time-dependent self-consistent field methods with dynamic magnetic fields

Cite as: J. Chem. Phys. 159, 104102 (2023); doi: 10.1063/5.0160317

Submitted: 31 May 2023 • Accepted: 11 August 2023 •

Published Online: 8 September 2023



View Online



Export Citation



CrossMark

Meilani Wibowo-Teale,^{1,a)} Benjamin J. Ennifer,¹ and Andrew M. Wibowo-Teale^{1,2,b)}

AFFILIATIONS

¹School of Chemistry, University of Nottingham, University Park, Nottingham NG7 2RD, United Kingdom

²Hylleraas Centre for Quantum Molecular Sciences, Department of Chemistry, University of Oslo, P.O. Box 1033 Blindern, N-0315 Oslo, Norway

^{a)} Author to whom correspondence should be addressed: meilani.wibowo@nottingham.ac.uk

^{b)} Electronic mail: andrew.teale@nottingham.ac.uk

ABSTRACT

The first finite basis set implementation of the real-time time-dependent self-consistent field method in a dynamic (time-dependent) magnetic field using London atomic orbitals (LAOs) is presented. The accuracy of the finite basis approach using LAOs is benchmarked against numerical results from the literature for the hydrogen atom and H₂ in the presence of rapidly oscillating magnetic fields. This comparison is used to inform the choice of appropriate basis sets for studies under such conditions. Remarkably, relatively modest compact LAO basis sets are sufficient to obtain accurate results. Analysis of electron dynamics in the hydrogen atom shows that LAO calculations correctly capture the time evolution of orbital occupations. The Fourier transformation of the autocorrelation function yields a power spectrum exhibiting harmonics associated with coherent emission, which closely matches the literature and further confirms the accuracy of this approach. The dynamical response of the electron density in H₂ for a magnetic field parallel to the internuclear axis shows similar behavior to benchmark studies. The flexibility of this implementation is then demonstrated by considering how the dynamical response changes as a function of the orientation of the molecule relative to the applied field. At non-parallel orientations, the symmetry of the system is lowered and numerical benchmark data, which exploit cylindrical symmetry, are no-longer readily available. The present study demonstrates the utility of LAO-based calculations for extreme dynamic magnetic fields, providing a stress-test on the choice of basis. Future applications of this approach for less extreme dynamic magnetic fields are briefly discussed.

© 2023 Author(s). All article content, except where otherwise noted, is licensed under a Creative Commons Attribution (CC BY) license (<http://creativecommons.org/licenses/by/4.0/>). <https://doi.org/10.1063/5.0160317>

I. INTRODUCTION

The electronic structure of atoms and molecules exhibits dramatic changes under strong time-independent (static) magnetic fields,^{1–37} where one atomic unit of magnetic field strength corresponds to $1B_0 \approx 2.35 \times 10^5$ T. For atoms and small molecules in the weak-field regime ($B \ll B_0$), the effects of the external field are small compared with the Coulomb interactions of the electrons and nuclei. In this regime, perturbation theory is often used to effectively describe the electronic structure and properties of atoms and molecules. However, as the field strength increases, perturbation theory can no longer be applied. In the extreme limit of ultra-strong fields $B \gg B_0$, known as the Landau regime, the effects of the field dominate over the Coulomb interactions and these may be regarded as a perturbation, leading to a theoretically simple, if less chemically

familiar, picture. In fact, for fields of the order of 10^2 – $10^6 B_0$ found on neutron stars and magnetars, theoretical predictions suggest that atoms are squeezed into cylindrical needle-like shapes and the familiar terrestrial chemistry, governed by Coulomb interactions, is lost. In between the weak-field and Landau regimes is the intermediate regime ($B \approx B_0$) in which the Coulomb interactions of the electrons are in competition with the effects of the applied field, and therefore, the interaction with the magnetic field cannot be treated using perturbation theory. Fields in the intermediate regime exist in the vicinity of magnetic white dwarf stars,³⁸ which can have fields with strengths of the order of B_0 .

The intermediate regime is of particular interest since there is a delicate interplay between all contributions to the electronic Hamiltonian. In particular, the paramagnetic spin and orbital Zeeman terms are counterbalanced by the diamagnetic field contribution,

and together, these effects are of similar importance to the electronic terms in the conventional molecular Hamiltonian. The influence of each term depends on the electronic state considered and the strength of the external magnetic field. For example, paramagnetic states initially decrease in energy as the magnetic field strength increases due to the Zeeman terms, which depend linearly on the magnetic field. However, they eventually rise in energy at high fields since the diamagnetic term has a quadratic dependence on the field. This gives rise to para- to diamagnetic transitions for such states. In contrast, the energy of diamagnetic states will rise as the field strength increases, and as a result, the electronic states reorder significantly with changes in the applied field. As the applied field strength changes, many different states may become the ground state for a given interval in the field strength.^{29,31,32,34} Even for simple atomic species, this gives rise to a much richer chemistry with frequent changes in the ground state electronic configuration and significant changes in properties of both the ground and excited states as a function of the applied field (see, e.g., Ref. 35). For molecular systems, the picture is even more complex since each electronic state will also exhibit a preferential orientation of the molecular frame with respect to the direction of the external magnetic field.^{29,31,34,37}

In the majority of studies, static magnetic fields have been considered. However, the use of strong time-dependent magnetic fields has been investigated for few-electron atoms and molecules by solving the time-dependent Schrödinger equation numerically in cylindrical coordinates.^{39–42} The electron dynamics of these systems then has been explored, revealing interesting exotic phenomena. For example, a continuous time-dependent magnetic field can drive population and depopulation of excited states in the hydrogen atom, indicating the possibility of coherent emission of photons with the associated harmonics appearing in the calculated photoemission spectrum under these conditions.⁴⁰

The focus of the present work is to extend the implementation of real-time time-dependent self-consistent field (RT-TDSCF) methods described in Ref. 31 to include the effects of time-dependent magnetic fields. The numerical studies of Refs. 40 and 42 provide important benchmark data against which this finite London atomic orbital (LAO) basis implementation can be assessed. It is well known that in strong time-dependent electric fields phenomena such as high-harmonic generation involve coherent excitation processes that require very careful choice of basis sets with care required to ensure adequate description of electronic states close to the continuum.⁴³ In this work, we will investigate the basis requirements to describe analogous processes with strong dynamic magnetic fields.

We begin by reviewing the theoretical foundations of the LAO-based real-time methods in Sec. II, introducing the modifications necessary for a time-dependent external magnetic field. In Sec. III A, we compare our finite basis LAO results with the numerical benchmark of Ref. 40, highlighting how to choose appropriate basis functions to describe the complex dynamics in strong time-dependent magnetic fields. The finite basis approach is then applied to compute the photoemission spectra and associated electron dynamics of the hydrogen atom and the H₂ molecule in a time-dependent strong magnetic field in Secs. III A and III B. For the H₂ molecule, the dynamics is also investigated for a range of orientations of the magnetic field relative to the internuclear axis, going beyond the scope of previously presented numerical approaches, which are limited to the parallel direction of the applied magnetic field where cylindrical

symmetry can be exploited. Concluding remarks and directions for future work are given in Sec. IV.

II. BACKGROUND AND THEORY

In this section, we present the theoretical foundations for our implementation of RT-TDSCF methods in a time-dependent magnetic field. Atomic units are used throughout the paper, unless otherwise specified. We commence in Sec. II A with a brief review of the basic equations for RT-TDSCF methods, introducing the modifications required for a time-dependent magnetic field. The particular choice of time-dependent magnetic field is then discussed in Sec. II B. In Sec. II C, the quantities used to analyze the dynamical response of atoms and molecules under these conditions are introduced along with the approach to calculate photoemission spectra from the RT-TDSCF trajectories.

A. Real-time time-dependent self-consistent field methods

In RT-TDSCF approaches, we consider the time-dependent Schrödinger equation

$$i \frac{\partial}{\partial t} \Psi(\mathbf{r}, t) = \hat{H}(\mathbf{r}, t) \Psi(\mathbf{r}, t), \quad (1)$$

where i is the imaginary unit, t is the time variable and $\Psi(\mathbf{r}, t)$ and $\hat{H}(\mathbf{r}, t)$ are the time-dependent wave function and Hamiltonian operator, respectively. The time-dependent SCF wave function is defined as a single Slater determinant constructed from the time-dependent one-electron orbitals $\phi_i(\mathbf{r}, t)$,

$$\Psi(\mathbf{r}, t) = \hat{A}[\phi_1(\mathbf{r}, t)\phi_2(\mathbf{r}, t) \dots \phi_i(\mathbf{r}, t)], \quad (2)$$

which can be written as a linear combination of time-independent basis functions $\chi_\mu(\mathbf{B}, \mathbf{r})$ and time-dependent coefficients $c_{\mu,i}(t)$,

$$\phi_i(\mathbf{r}, t) = \sum_{\mu} c_{\mu,i}(t) \chi_{\mu}(\mathbf{B}, \mathbf{r}). \quad (3)$$

Here, we use a basis set of London atomic orbitals (LAOs),⁴⁴ which have an explicit dependence on the external magnetic field \mathbf{B} and are defined as

$$\chi_{\mu}(\mathbf{B}, \mathbf{r}) = \tilde{\chi}_{\mu}(\mathbf{r}) \exp \left[-\frac{i}{2} \mathbf{B} \times (\mathbf{A} - \mathbf{O}) \cdot \mathbf{r} \right]. \quad (4)$$

The function $\tilde{\chi}_{\mu}(\mathbf{r})$ is a conventional basis function (in this work a Gaussian), centered at the position $\mathbf{A} = (A_x, A_y, A_z)$, and \mathbf{O} is the gauge-origin associated with the magnetic field. This choice of basis ensures that calculated results are independent of the arbitrary choice of gauge-origin, \mathbf{O} .

The time-dependent density matrix can be constructed at each time step as

$$P'_{\mu\nu}(t) = \sum_i c_{\mu,i}^*(t) c_{\nu,i}(t), \quad (5)$$

where the prime denotes the quantity is in the atomic orbital (AO) basis. The corresponding Fock matrix at a given time t is then constructed as

$$F'_{\mu\nu}(\mathbf{B}, t) = \langle \chi_{\mu}(\mathbf{B}, r) | \hat{F}(\mathbf{B}, t) | \chi_{\nu}(\mathbf{B}, r) \rangle, \quad (6)$$

where $\hat{F}(\mathbf{B}, t)$ is the Fock operator (or Kohn–Sham effective Hamiltonian) in a magnetic field \mathbf{B} at time t , see, e.g., Ref. 31 for further details. Here, we note that now since the basis functions carry an explicit dependence on the magnetic field then all (one and two-electron) integrals must be recalculated at each time step—necessitating the use of integral-direct algorithms for the Fock matrix construction.⁴⁵ In the notation throughout this paper, we use \mathbf{B} to represent the field at time t , $\mathbf{B}(t)$.

The time propagation in Eq. (1) is most conveniently carried out in an orthonormal AO basis. Since the basis functions are generally not orthonormal, the overlap matrix can be evaluated as

$$S_{\mu\nu}(\mathbf{B}) = \langle \chi_\mu(\mathbf{B}, r) | \chi_\nu(\mathbf{B}, r) \rangle \quad (7)$$

and used to transform the time-dependent density and Fock matrices to an orthonormal basis using the Löwdin orthonormalization,

$$\mathbf{P}(\mathbf{B}, t) = \mathbf{S}^{1/2}(\mathbf{B}) \mathbf{P}'(t) \mathbf{S}^{1/2}(\mathbf{B})^\dagger, \quad (8)$$

$$\mathbf{F}(\mathbf{B}, t) = \mathbf{S}^{-1/2}(\mathbf{B})^\dagger \mathbf{F}'(\mathbf{B}, t) \mathbf{S}^{-1/2}(\mathbf{B}). \quad (9)$$

Here, we see that since the basis functions are field dependent then in a time-dependent magnetic field the orthogonalization matrix must be updated at each time step and the density matrix in the orthonormal basis $\mathbf{P}(\mathbf{B}, t)$ therefore inherits a dependence on the magnetic field.

In an orthonormal basis, the Liouville–von Neumann equation, which describes the time evolution of the density matrix, can then be expressed as

$$i \frac{\partial \mathbf{P}(\mathbf{B}, t)}{\partial t} = [\mathbf{F}(\mathbf{B}, t), \mathbf{P}(\mathbf{B}, t)], \quad (10)$$

and formally, its solution can be written in terms of a unitary propagator

$$\mathbf{P}(\mathbf{B}, t) = \mathbf{U}(\mathbf{B}, t, 0) \mathbf{P}(\mathbf{B}, 0) \mathbf{U}^\dagger(\mathbf{B}, t, 0), \quad (11)$$

where

$$\mathbf{U}(\mathbf{B}, t_2, t_1) = \hat{\mathcal{T}} \exp \left(-i \int_{t_1}^{t_2} \mathbf{F}(\mathbf{B}, t) dt \right) \quad (12)$$

involves time-ordered integration (denoted by $\hat{\mathcal{T}}$). Since \mathbf{U} is unitary, then properties present in $\mathbf{P}(\mathbf{B}, 0)$, such as idempotency and trace (particle number), are preserved for times $t > 0$. In practice, Eq. (10) is solved by discretizing time into small time steps Δt such that the propagator at time step N is described by $\mathbf{U}_N = \mathbf{U}(\mathbf{B}, t_N + \Delta t, t_N)$ and propagates $\mathbf{P}(\mathbf{B}, t)$ to $\mathbf{P}(\mathbf{B}, t + \Delta t)$.

In this work, we use the unitary propagator based on the second-order Magnus expansion (Magnus2), approximated using the trapezoidal rule as

$$\mathbf{U}(\mathbf{B}, t + \Delta t, t) \approx \exp \left(-\frac{i\Delta t}{2} [\mathbf{F}(\mathbf{B}, t) + \mathbf{F}(\mathbf{B}, t + \Delta t)] \right), \quad (13)$$

where at a given time step $\mathbf{F}(\mathbf{B}, t)$ is evaluated from density matrix $\mathbf{P}(\mathbf{B}, t)$ and then an approximate density matrix $\hat{\mathbf{P}}(\mathbf{B}, t + \Delta t)$ is evaluated using the simple Euler approximation $\hat{\mathbf{P}}(\mathbf{B}, t + \Delta t) = [-i\Delta t \mathbf{F}(\mathbf{B}, t)] \mathbf{P}(\mathbf{B}, t) [-i\Delta t \mathbf{F}(\mathbf{B}, t)]^\dagger$; this density

matrix is then used to evaluate $\mathbf{F}(\mathbf{B}, t + \Delta t)$ and Eq. (13) from which the resulting \mathbf{U} is then used for the final propagation of the density matrix to generate $\mathbf{P}(\mathbf{B}, t + \Delta t)$ for the next time step. This procedure requires two Fock matrix constructions and two matrix exponential evaluations per time step. The errors in this approach are $\mathcal{O}(\Delta t^2)$, and in our experience, the integration is stable for modest time steps up to 0.20 a.u.³¹ Several alternative propagation algorithms have been implemented in QUEST,⁴⁶ and their efficiency and stability has been assessed and presented in Ref. 31.

B. Time-dependent magnetic field

The time-dependent magnetic field is modeled as a linear-ramped sinusoidal function, modulating a spatially uniform magnetic field with maximum amplitude $|\mathbf{B}_{\max}|$,

$$\mathbf{B}(t) = \mathbf{B}_{\max} f(t) \sin(\omega t), \quad (14)$$

where ω is the magnetic-field frequency and $f(t)$ is the ramp function, defined as

$$f(t) = \begin{cases} t/t_0 & \text{for } t \leq t_0, \\ 1 & \text{otherwise.} \end{cases} \quad (15)$$

Here, t_0 is the time required for the magnetic field to reach its maximum value \mathbf{B}_{\max} . The ramp function $f(t)$ is used to prevent a sudden increase in the magnetic-field strength and also facilitates comparison with previous studies.^{40,47,48}

C. Photoemission spectra and electron dynamics

The electron dynamics of atoms and molecules in the time-dependent magnetic field can be characterized by examining the time evolution of orbital occupation numbers—indicating which orbitals become significantly populated at times $t > 0$. These occupation numbers are calculated by projecting the time-dependent density matrix $\mathbf{P}(\mathbf{B}, t)$ onto the molecular orbital coefficients for each orbital $\mathbf{C}_k(0)$ at time $t = 0$,

$$n_k = \mathbf{C}_k^\dagger(0) \mathbf{P}(t) \mathbf{C}_k(0). \quad (16)$$

To calculate the photoemission spectra, the ground state complex autocorrelation function

$$\tilde{\mathbf{C}}(t) = \langle \Psi(0) | \Psi(t) \rangle \quad (17)$$

is computed at each time step in the trajectory, where $\Psi(0)$ and $\Psi(t)$ are the ground state wave function at time $t = 0$ and at times $t > 0$. This quantity is a measure of the overlap of the wave function at time t with the initial wave function.

The autocorrelation function between two Slater determinants can be written in terms of the determinant of the overlap matrix transformed into molecular orbital basis.⁴⁹ In the present case, it should be noted that since the LAOs depend explicitly on the magnetic field and this changes between time steps, we must evaluate the mixed overlap matrix

$$S''_{\mu\nu} = \langle \chi_\mu(\mathbf{B}(0)) | \tilde{\chi}_\nu(\mathbf{B}(t)) \rangle. \quad (18)$$

In particular, while the dimensions μ and ν are of the same size with common Gaussian contributions $\tilde{\chi}_\mu(\mathbf{r})$ in Eq. (4), the London phase

factors for the LAOs at time $t = 0$ and at times $t > 0$ will differ. This is indicated by a tilde on the functions in the ket to emphasize the different basis. The double prime is then used to indicate that this quantity is in a mixed AO basis. The autocorrelation function can then be evaluated as

$$\tilde{C}(t) = \det [C(0)S''C(t)], \quad (19)$$

where $C(0)$ and $C(t)$ are the occupied molecular orbital coefficients at time $t = 0$ and at times $t > 0$, respectively. The photoemission spectra can then be calculated by Fourier transformation of the autocorrelation function,

$$C(\Omega) = \text{Re} \left[\int_{t_0}^t \exp(-i\Omega t) \tilde{C}(t) dt \right]. \quad (20)$$

III. RESULTS AND DISCUSSION

The RT-TDSCF method in a time-dependent magnetic field described in Sec. II has been implemented in our program QUEST⁴⁶ and used to perform real-time calculations of the hydrogen atom and the H₂ molecule in a strong time-dependent magnetic field. We first consider the choice of the basis set and time step for RT-TDSCF calculations on the hydrogen atom, comparing the results with the grid-based method reported in Ref. 40. Calculations of the dynamical response of the H₂ molecule in a time-dependent magnetic field parallel to the internuclear axis and the associated photoemission spectra are then performed using a choice of time step, simulation and basis set informed by this comparison. The effect of orientation of the internuclear axes relative to the magnetic field on the observed dynamical response is then examined.

A. Basis-set dependence and comparison with literature

For one-electron systems, such as the hydrogen atom, Hartree-Fock (HF) theory is exact. Therefore, any deviation from numerical grid-based results is solely due to the use of a finite basis set. To investigate the basis set dependence and the effect of the integration time step for RT-TDHF calculations in a time-dependent magnetic field with the incident frequency $\omega = 0.048$ a.u. and $|\mathbf{B}_{\max}| = 2.0B_0$, we performed RT-TDHF calculations for the hydrogen atom using the Magnus2 propagator algorithm employing two different basis sets—aug-cc-pVDZ and aug-cc-pVTZ, in conjunction with two different integration time steps, $\Delta t_S = 0.035$ a.u. (0.85 as) and $\Delta t_L = 0.1$ a.u. (2.42 as). In each case, the total simulation time is maintained at ~ 240 fs. The small integration time step Δt_S was chosen in order to compare our results with the grid-based method presented in Ref. 40, which also describes how the incident frequency was selected. Throughout the calculations in the present work, the electric field induced by the oscillating magnetic field is ignored since it may be considered a weak perturbation in comparison to the magnetic field for $|\mathbf{B}_{\max}|$ of the order of B_0 ; see Ref. 40 for further details.

1. Photoemission spectrum

Figure 1 shows the computed photoemission spectra of the hydrogen atom using $\Delta t_S = 0.035$ a.u. in the aug-cc-pVDZ and aug-cc-pVTZ basis sets. Both spectra exhibit a doublet structure,

consistent with Ref. 40. The doublet structure arises because the Hamiltonian contains terms that are both linear and quadratic in \mathbf{B} . The field has a sinusoidal time-dependence with frequency ω , and the quadratic terms give rise to contributions with frequency 2ω . The Floquet theorem can be used to express the resulting time-dependent wavefunction as a linear combination of functions that are periodic in time with complex phase factors. As a consequence, the Fourier transform of the complex autocorrelation function of Eq. (19) shows spectral frequencies at multiples of the magnetic-field frequency plus the Floquet quasi-energies,^{40,50} leading to the observed doublet structure.

The photoemission spectrum in the aug-cc-pVDZ basis displays both odd and even order harmonics—differing qualitatively from both the aug-cc-pVTZ basis spectra and that in Ref. 40, where only even order harmonics are observed. The origin of this discrepancy can be determined by considering the dynamical response of the system to the time-dependent magnetic field. Figures 2(a) and 3(a) show the 1s orbital populations for the hydrogen atom in each basis set. Both produce a similar qualitative behavior; however, in the smaller aug-cc-pVDZ basis set, the electron dynamics occurs over a shorter time period $T_d = 780 \pm 120$ a.u.—significantly faster than the dynamics seen in Fig. 3 and Ref. 40. Examination of the occupation numbers for the higher-energy orbitals using Eq. (16) reveals that this difference occurs due to the lack of d-orbitals in the smaller basis set, in particular the d_{z^2} orbital, which is significantly populated in the larger aug-cc-pVTZ basis set simulations (compare Figs. 2 and 3).

From this analysis, it is clear that for the hydrogen atom higher angular momentum basis functions are a requirement in order to capture the correct harmonics and doublet structure in the computed photoemission spectrum and the associated dynamics. As a

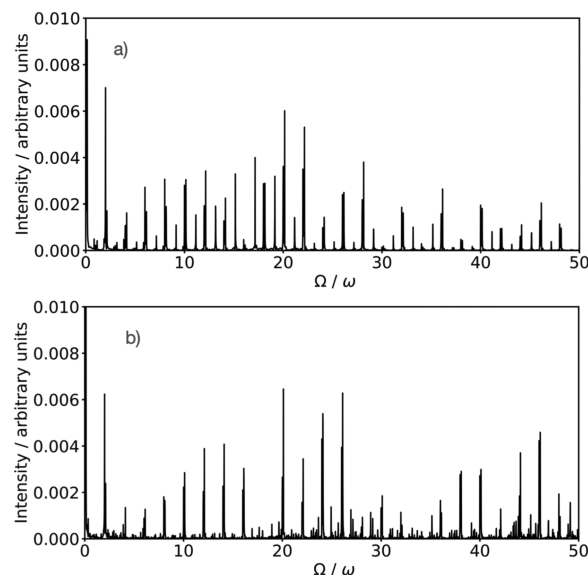


FIG. 1. Computed photoemission spectrum of the hydrogen atom using the (a) aug-cc-pVDZ and (b) aug-cc-pVTZ basis sets, obtained using integration time step $\Delta t_S = 0.035$ a.u. Intensities are scaled with the incident frequency of the time-dependent magnetic field $\omega = 0.048$ a.u.

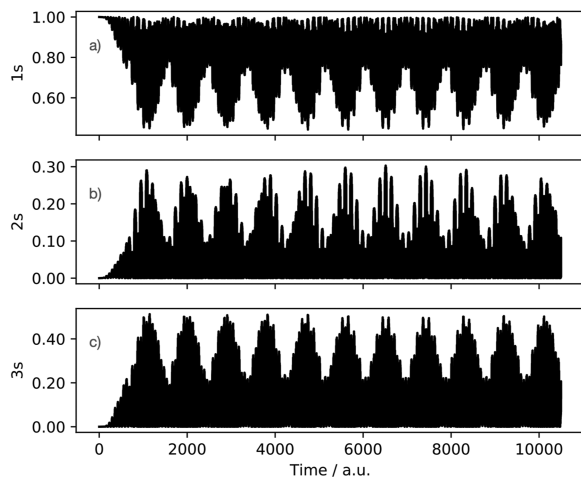


FIG. 2. Orbital occupation numbers of the (a) 1s, (b) 2s, and (c) 3s orbitals of the hydrogen atom, obtained at the RT-TDHF/aug-cc-pVDZ level with integration time step $\Delta t_S = 0.035$ a.u. Only orbitals with quantum number $m = 0$ are shown as they become populated during the propagation. The p-orbitals are not shown as they remain unpopulated.

result, the standard aug-cc-pVDZ basis is inadequate for calculations under these extreme conditions.

2. Electron dynamics

Figure 3 shows the orbital occupation numbers of the 1s, 2s, 3s, $3d_{z^2}$, 4s, and 5s orbitals under a strong time-dependent oscillating magnetic field at the RT-TDHF/aug-cc-pVTZ level with integration time step $\Delta t_S = 0.035$ a.u. Due to the symmetry imposed by the field, only orbitals with the quantum number $m = 0$ are populated during the course of simulation while p-orbitals remain unpopulated. During the dynamics, the population of the 1s orbital oscillates between 1.0 and 0.5 with a time period ~ 1200 a.u. while the populations of the higher-energy 2s, 3s, $3d_{z^2}$, 4s, and 5s orbitals start at zero and oscillate with the opposite phase to the 1s orbital—conserving the total particle number. The orbital occupation numbers show a long timescale dynamics with a time period $T_d = 1200 \pm 150$ a.u., which is approximately ten times longer than the period of the oscillating magnetic field (~ 130 a.u.). This is in good agreement with the observations presented in Ref. 40 and significantly longer than that obtained with the smaller aug-cc-pVDZ basis set.

In the presence of a time-dependent oscillating magnetic field in the hydrogen atom, the electron is transferred continuously between the ground and excited states in an oscillatory manner, as shown in Fig. 3, demonstrating that during the dynamics the excited states are being populated and depopulated. This behavior indicates the occurrence of coherent excitation and de-excitation—consistent with the photoemission spectrum of Fig. 1(b). This spectrum can be interpreted as the frequency distribution of the emitted photon—analogue to the high-harmonic generation process in the case of strong interaction between the atom and intense laser field.

It is noteworthy that the basis set requirements for the coherent response in strong time-dependent magnetic fields are somewhat different to those for high-harmonic generation. In particular, the

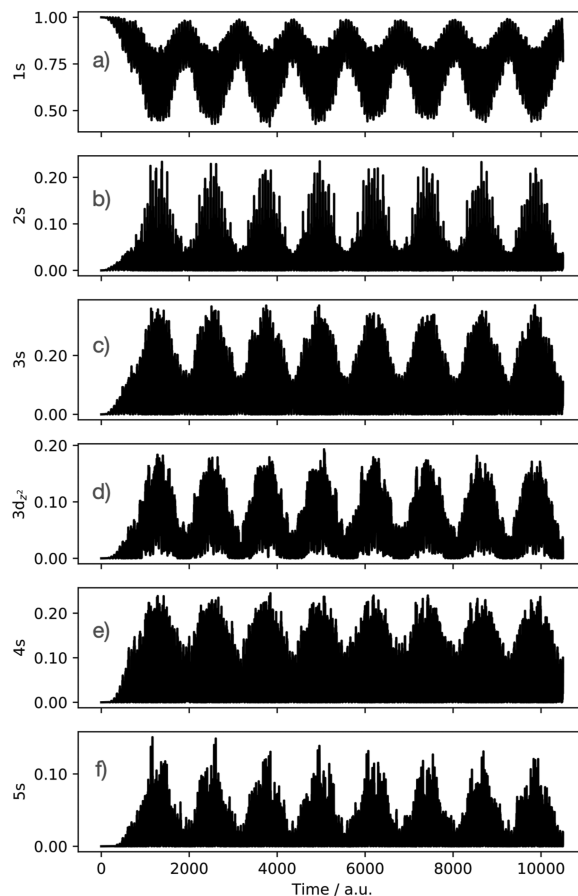


FIG. 3. Orbital occupation numbers of the (a) 1s, (b) 2s, (c) 3s, (d) $3d_{z^2}$, (e) 4s, and (f) 5s orbitals of the hydrogen atom, obtained at the RT-TDHF/aug-cc-pVTZ level with integration time step $\Delta t_S = 0.035$ a.u. Only orbitals with quantum number $m = 0$ are shown as they become populated during the propagation. The p-orbitals are not shown as they remain unpopulated.

dynamics involves significant population of less high-lying orbitals, and so, very diffuse basis functions and functions designed to help model near-continuum states are not required. However, the transitions in the presence of the magnetic field do necessitate a good description of higher angular momentum orbitals—for example, the $3d_{z^2}$ orbital—which can be involved in the dynamics. These simple observations can be used to guide the selection of appropriate basis sets for other systems under these conditions with relatively compact standard basis sets being sufficient.

3. Computational efficiency

The inclusion of a time-dependent magnetic field in real-time calculations increases the cost of the simulation since it becomes necessary to evaluate all integrals in a direct manner at every time step. This is exacerbated when a small integration time step is used since the calculation time scales linearly with the number of time steps. However, as reported in Ref. 31, the Magnus2 propagation algorithm is relatively stable for much larger integration time steps of up to 0.2 a.u. both in the absence and presence of a static magnetic

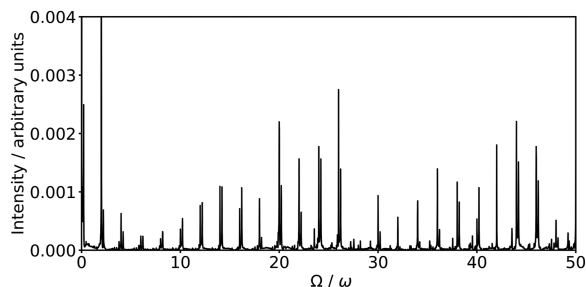


FIG. 4. Computed photoemission spectrum of the hydrogen atom, obtained at the RT-TDHF/aug-cc-pVTZ level with integration time step $\Delta t_L = 0.1$ a.u. Intensities are scaled with the frequency of the time-dependent magnetic field, $\omega = 0.048$ a.u.

field regardless the level of theory. In particular, the combination of the Magnus2 propagation algorithm with a modest integration time step of 0.1 a.u. displays a good trade-off between accuracy and efficiency of the real-time simulations of absorption spectra for strong static magnetic fields. We have therefore investigated the use of a larger time step $\Delta t_L = 0.1$ a.u. to significantly reduce the cost of real-time simulations, reducing total number of steps required for the same total simulation time.

Figure 4 shows the computed photoemission spectrum of the hydrogen atom, obtained at the RT-TDHF/aug-cc-pVTZ level with a time step $\Delta t_L = 0.1$ a.u. This spectrum recovers essentially the same information as that obtained using a smaller time step $\Delta t_S = 0.035$ a.u. [compare with Fig. 1(b)]. The even harmonics and doublet structure are clearly well reproduced. However, absolute intensities are somewhat different, which may be expected as these are slowly convergent with respect to the timestep size in RT simulations. Nonetheless, relative intensities of the peaks remain broadly similar. Overall, this approach reduces the overall cost by a factor of 3 without significantly impacting the quality of the spectrum. A second significant factor in managing the cost of real-time simulations is the total duration. From the dynamical response in Fig. 3, it can be observed that beyond 6000 a.u. of time no significant further changes in the dynamics are observed. Truncating the simulation to this duration also yields a photoemission spectrum that is almost indistinguishable from that in Fig. 4.

B. The H_2 molecule

We now examine the response of the H_2 molecule in a time-dependent magnetic field modeled using Eqs. (14) and (15), defined in Sec. II B. This system was previously studied in Ref. 51 for parallel orientation of the magnetic field relative to the internuclear axis. The maximum strength of the time-dependent magnetic field was varied from $|\mathbf{B}_{\max}| = 0.4\text{--}1.0B_0$ with the incident frequency $\omega = 0.767$ a.u. The time-dependent magnetic field was ramped over a period of five magnetic-field cycles (one cycle corresponds to $2\pi/\omega$), which corresponds to $t_0 \approx 41$ a.u. The RT-TDHF calculations were carried using the Magnus2 propagator algorithm employing the aug-cc-pVTZ basis set for a total simulation time of 100 magnetic cycles (820 a.u. of time). This long duration was chosen in order to capture all significant physical changes in the H_2 molecule under the strong oscillating time-dependent magnetic field and allows direct

comparison with the results of Ref. 51; further discussion of how the simulation parameters were selected can also be found in this reference. Here, we again consider RT-TDHF since for few-electron systems the errors associated with density-functional approximations can outweigh the benefits of the approximate inclusion of electron correlation effects, see, e.g., Ref. 37 for a recent discussion of this point.

1. Magnetic field strength: Parallel magnetic fields with $|\mathbf{B}_{\max}| = 0.4\text{--}1.0B_0$

We commence by analyzing the electron dynamics of the H_2 molecule in a parallel time-dependent magnetic field (B_{\parallel}) for $|\mathbf{B}_{\max}| = 0.4, 0.6, 0.8,$ and $1.0B_0$; see Fig. 5. In the absence of a magnetic field, the point group of the H_2 molecule is $D_{\infty h}$ and the lowest occupied orbital is the $1\sigma_g^+$. In the presence of a magnetic field, the unitary point group is reduced to an Abelian subgroup that comprises the symmetry operations present in both the zero-field molecular point group and that of a uniform magnetic field $C_{\infty h}$. In general, only rotation axes parallel to the field, mirror planes perpendicular to the field and the center of inversion, if present, will remain.^{33,52} More generally, a complete characterization of the symmetry of a system in a magnetic field may require consideration of time-reversal symmetry, and certain anti-unitary transformations may also be symmetry transformations of the combined molecule and field,^{53–55} requiring the use of magnetic groups and corepresentations instead of representations.^{56–58} See, for example, Ref. 36 for a recent further discussion.

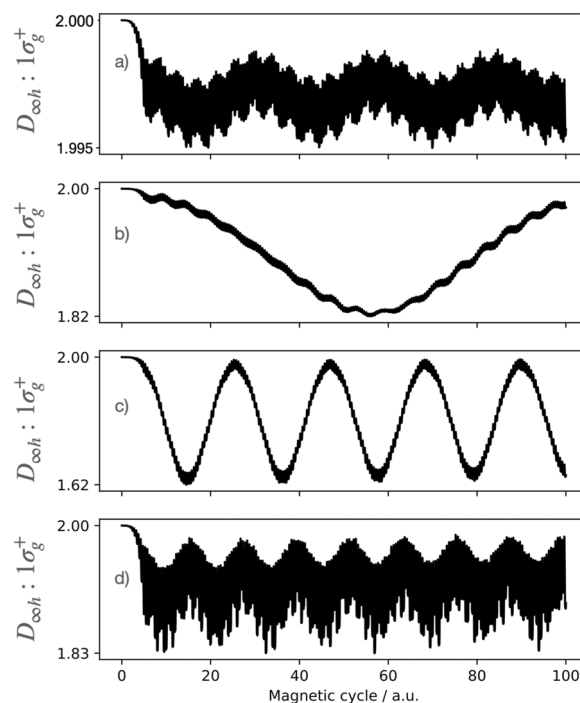


FIG. 5. The $1\sigma_g^+$ orbital populations of the H_2 molecule in a parallel time-dependent magnetic field (B_{\parallel}) for $|\mathbf{B}_{\max}| = 0.4, 0.6, 0.8,$ and $1.0B_0$ [(a)–(d), respectively], computed at the RT-TDHF/aug-cc-pVTZ level. Note that the same value of the incident frequency of the time-dependent magnetic field $\omega = 0.767$ a.u. is used.

In the present work, we consider the occupation numbers in terms of the projection onto the $t = 0$ initial orbitals as described by Eq. (16). Since the field is ramped and the initial orbitals are evaluated at $\mathbf{B} = 0$, we will use the zero-field symmetry labels for these contributions. In addition, we consider how these orbitals evolve as a function of field and, where appropriate, label the corresponding orbitals in a field according to the reduced unitary symmetry in the presence of the field. For the parallel field orientation, the reduction in symmetry is relatively modest; the point group changes from $D_{\infty h}$ to $C_{\infty h}$ with the lowest occupied molecular orbital becoming $1\sigma_g$. Throughout this work, all symmetry labels have been deduced automatically using the QSYM² program, part of the QUEST program package.⁴⁶

In Fig. 5, it can be observed that in the parallel magnetic field (B_{\parallel}) with $|\mathbf{B}_{\max}| = 0.4B_0$ the electrons remain in the ground state. As the maximum magnetic-field strength increases, the $1\sigma_g^+$ orbital starts to depopulate and re-populate in an oscillatory manner. The largest population changes occur at the maximum magnetic-field strength $|\mathbf{B}_{\max}| = 0.8B_0$. In this case, the $1\sigma_g^+$ orbital population oscillates between 2.00 and 1.62 with a time period of ~ 20 magnetic cycles—indicating the near-resonance excitation for the H_2 molecule in a strong oscillating time-dependent magnetic field. For the time-dependent magnetic fields with maximum strengths $|\mathbf{B}_{\max}| = 0.6$ and $1.0B_0$, the depopulation of electrons in the $1\sigma_g^+$ orbital is weaker—the population of the $1\sigma_g^+$ orbital oscillates between 2.00 and 1.82 with time periods of about 100 and 12 magnetic cycles, respectively. This analysis demonstrates that the near-resonance excitation for the H_2 molecule in a time-dependent magnetic field can be controlled by tuning the magnetic field strength. In the following, we focus on the dynamical response of the electrons in a parallel magnetic field (B_{\parallel}) for $\mathbf{B}_{\max} = 0.8B_0$ —corresponding to the near-resonance excitation for the H_2 molecule in a strong oscillating time-dependent magnetic field.

A significant complexity in the presence of a magnetic field is that the orbital energies significantly reorder for $|\mathbf{B}| > 0$. Degenerate π and δ orbitals split, and this strongly depends on both the strength and orientation of the applied magnetic field. The energies of the σ orbitals also change because of the changes in the electronic structure of a molecule in the presence of a magnetic field. In the present work, the field strength also varies as a function of the simulation time. To track the orbital energies and assignments as a function of magnetic field across the entire range of interest, we used the maximum-overlap method (MOM) to follow the evolution of the orbitals from those in the absence of a field through to $|\mathbf{B}_{\max}|$. Further details of this procedure are presented in Ref. 31.

Figure 6 shows the orbital populations for the lowest $1\sigma_g^+$ orbital and the five higher-lying orbitals with most significant population for the H_2 molecule in a parallel magnetic field (B_{\parallel}) with $|\mathbf{B}_{\max}| = 0.8B_0$, which are ordered according to their maximum population. The labels on the left correspond to the initial orbitals, labeled according to the $D_{\infty h}$ point group, while the labels on the right are for the corresponding orbitals in the presence of a parallel magnetic field with $|\mathbf{B}| = 0.8B_0$ with point group $C_{\infty h}$. In the parallel orientation, the reduction in symmetry is relatively minor, and so, the orbitals involved in the dynamics retain their σ -character.

During the dynamics, the electrons in the $1\sigma_g^+$ orbital are excited and de-excited continuously to and from the higher-lying

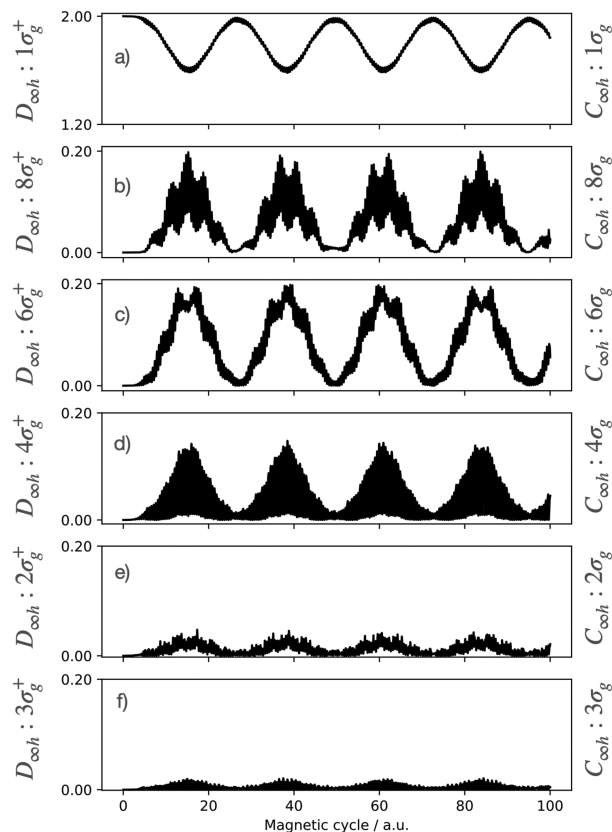


FIG. 6. The $1\sigma_g^+$ and higher-lying orbital populations [see Eq. (16)] for the H_2 molecule in a parallel time-dependent magnetic field (B_{\parallel}) for $|\mathbf{B}_{\max}| = 0.8B_0$, computed at the RT-TDHF/aug-cc-pVTZ level. The populations of the five higher-lying orbitals with most significant contribution to the dynamics are shown, ordered according to their maximum occupation number.

$2\sigma_g^+$, $3\sigma_g^+$, $4\sigma_g^+$, $6\sigma_g^+$, and $8\sigma_g^+$ orbitals—demonstrating the phenomenon of a coherent excitation and de-excitation. The population of the $1\sigma_g^+$ orbital starts at 2.00, equal to the number of electrons in the H_2 molecule, and during the dynamics, the population of this orbital decreases and reaches a minimum at ~ 1.62 with a time period of ~ 20 magnetic cycles. The populations of the higher-lying orbitals start at zero and oscillate with the opposite phase to the $1\sigma_g^+$ orbital—conserving the total number of electrons. The high-lying orbitals with highest population during the dynamics are the $8\sigma_g^+$, $6\sigma_g^+$, and $4\sigma_g^+$ orbitals. It should be noted that all of the orbitals involved in the dynamics are of *gerade* (g) character. This is because the allowed transitions from the $1\sigma_g^+$ ground state are determined by magnetic-dipole selection rules, which in the present case means that $g \leftrightarrow g$ transitions are allowed while $g \leftrightarrow u$ transitions are forbidden.

In the presence of an external magnetic field, molecular orbitals are generally complex functions, and so, their visualization is more challenging than in the absence of a field where the orbitals may be chosen real. Figure 7 shows contour plots of the square modulus of the molecular orbitals in the xz -plane of the H_2 molecule that are involved during the dynamics, evaluated in the absence of a

magnetic field (left panels), and the corresponding orbitals in a parallel magnetic field (B_{\parallel}) with field strength of $0.8B_0$ (right panels). In this case, the molecular axis of the H_2 molecule is the Cartesian z axis, coincident with direction of the applied magnetic field. In each case, an iso-surface plot is also shown as an inset (viewed down the y axis), where the color coding reflects the phase angle according to the color wheel shown in part (a) of each panel. In the presence of a parallel time-dependent magnetic field, the molecular orbitals change smoothly between those shown in the left-hand and right-hand panels of Fig. 7 during each magnetic cycle. For the parallel orientation of the magnetic field, the orbitals remain real throughout the dynamics; this is clearly visible in the inset iso-surfaces, where the red and blue colors of each lobe are along the real line in the color wheel. While this is expected for the parallel orientation with the London gauge-origin at the center of mass, complex orbitals are obtained for other orientations, as will be discussed in Sec. III B 2.

In a static parallel magnetic field, the electron density of the H_2 molecule contracts toward the internuclear axis slightly and this effect, although subtle, can be discerned by comparing parts (a) of the left and right panels of Fig. 7. However, in the presence of a time-dependent field, the population of the higher-lying molecular orbitals gives rise to more substantial fluctuations in the electron

density. In continuously driven time-dependent dynamical response calculations, it is customary to use a sufficiently long duration so that all significant physical changes during the dynamics can be captured. The dynamical responses and their interpretation in this case appear to have developed completely within 45 magnetic cycles, and the significant features of the electron dynamics after 45 magnetic cycles simply repeat due to the oscillatory manner of the dynamical response of the H_2 molecule (see Fig. 6). It is therefore sufficient to limit a detailed analysis and visualization of the electron density and density differences to the first 45 magnetic cycles.

The electron density of the H_2 molecule at different times (magnetic cycles) during the simulation is shown in Fig. S1 of the supplementary material. It is clear that none of the electron densities at magnetic cycles corresponding to $t > 0$ return to the original size and shape even when the time-dependent magnetic field vanishes temporarily at the full-cycle. Hence, the electron density deforms continuously despite the fact that the time-dependent magnetic field vanishes momentarily—preventing the electron density returning to its original size and shape at $t = 0$. For magnetic cycles 6 and 25, corresponding to the times at which the lowest $1\sigma_g^+$ orbital reaches its maximum population (see Fig. 6), the electron density remains slightly compressed in the direction orthogonal to the applied magnetic field (the Cartesian x axis). At magnetic cycle 14, where most

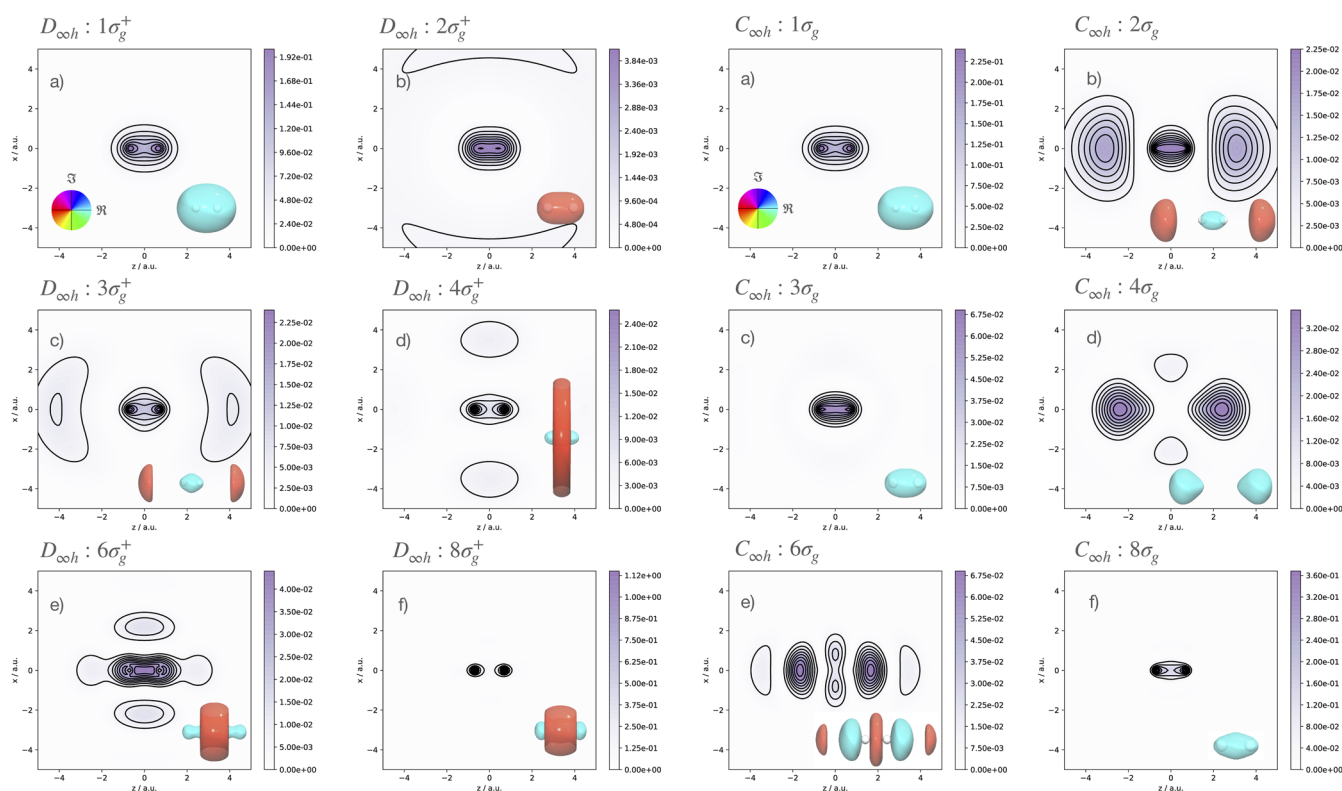


FIG. 7. The molecular orbitals that acquire significant population during the dynamics of the H_2 molecule in a time-dependent parallel magnetic field (B_{\parallel}) with $|\mathbf{B}_{\max}| = 0.8B_0$ according to the populations of Eq. (16). The orbitals are computed at the HF/aug-cc-pVTZ level in the absence of an external magnetic field [left panels (a)–(f)] and in a static parallel external magnetic field with $|\mathbf{B}| = 0.8B_0$ [right panels (a)–(f)]. Iso-surfaces of each orbital are shown as insets, color-coded according to the color wheel shown in panels (a). In the absence of a magnetic field, the point group is $D_{\infty h}$, which is reduced to $C_{\infty h}$ in the field.

of electrons are excited to high-lying molecular orbitals and the population of the lowest $1\sigma_g^+$ orbital reaches its minimum, the electron density appears to contract toward the nuclei.

In fact, the redistribution of the electron density due to the time-dependent magnetic field can be analyzed more clearly by computing the electron density difference

$$\Delta\rho(\mathbf{r}, t) = \rho(\mathbf{r}, t) - \rho(\mathbf{r}, 0), \quad (21)$$

where $\rho(\mathbf{r}, t)$ and $\rho(\mathbf{r}, 0)$ are the electron density at time t and $t = 0$, respectively. Figure 8 shows this quantity at magnetic cycles 6, 14, 25, and 35. The positive (red) and negative (blue) regions of $\Delta\rho(\mathbf{r}, t)$ indicate a transient accumulation and depletion of the electron density with respect to $t = 0$. For magnetic cycles 6 and 25, when the population of the lowest $1\sigma_g^+$ orbital is maximal, the density accumulates around the nuclei and in the regions closest to the z axis

and is depleted in regions far away from the nuclei on the x axis [see Figs. 8(a) and 8(c)]. This accumulation of density in the bonding region suggests that the strong oscillating time-dependent magnetic field induces a possibility of transient bond strengthening during the dynamics. Indeed, this is consistent with the observations from static magnetic-field calculations on the $^1\Sigma_g^+$ state in Ref. 14, where the equilibrium bond length was observed to decrease with increasing magnetic field.

In contrast, for magnetic cycles 14 and 35, when the population of the lowest $1\sigma_g^+$ orbital is minimal, the density difference plots show significant accumulations are located at relatively large distances along the x axis, perpendicular to the internuclear axis, as well as accumulations very close to the nuclei. The more distant regions mostly contain part of the high-lying $4\sigma_g^+$ and $6\sigma_g^+$ orbitals, see Fig. 7, which acquire significant population during the dynamics. The significant reduction in electron density in

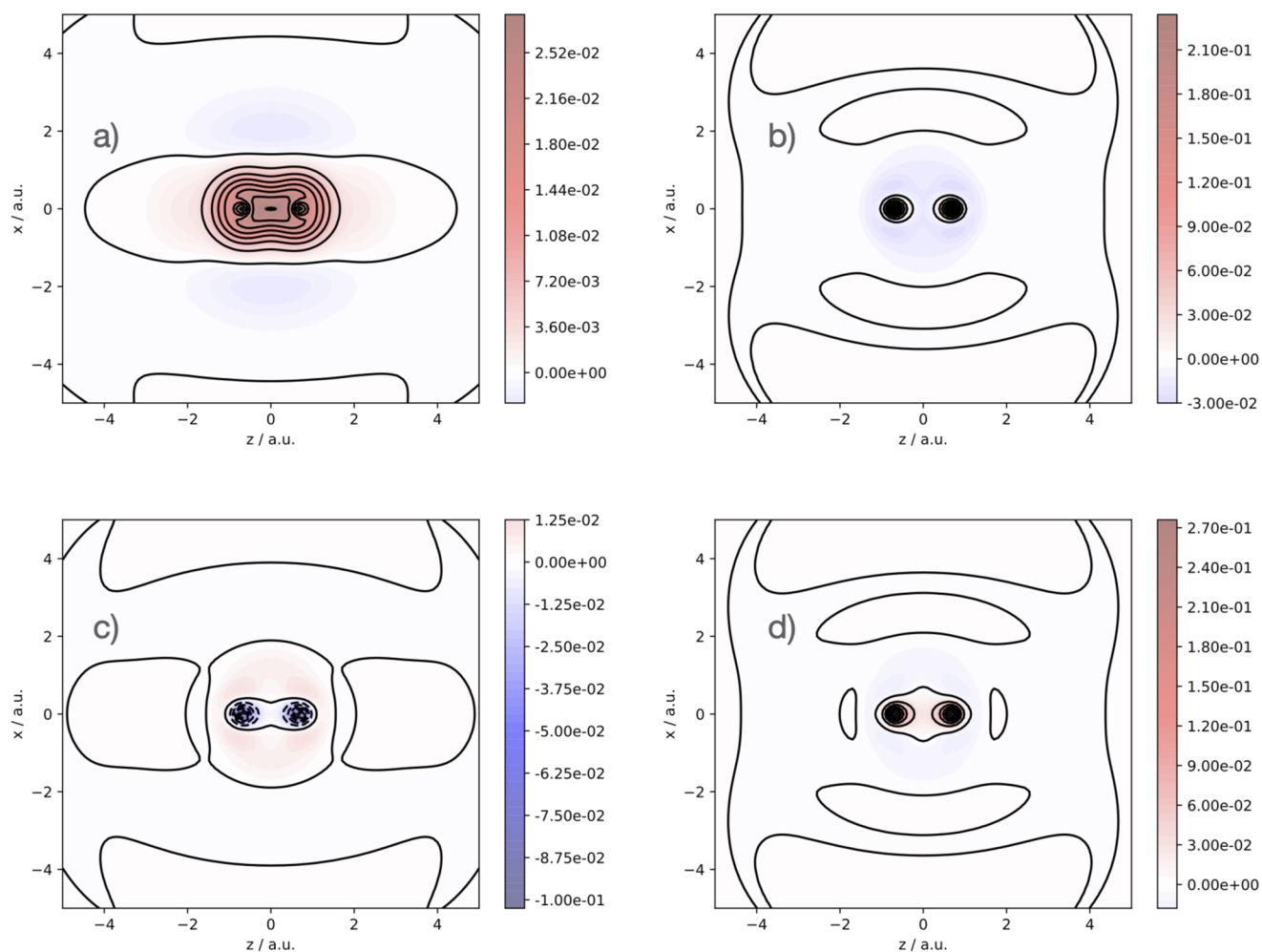


FIG. 8. Electron density difference ($\Delta\rho(\mathbf{r}, t)$) contours for the H_2 molecule at (a) 6, (b) 14, (c) 25, and (d) 35 magnetic cycles in a parallel time-dependent magnetic field (B_{\parallel}) with field strength of $0.8B_0$, computed at the RT-TDHF/aug-cc-pVTZ level. Note that the positive and negative values of $\Delta\rho(\mathbf{r}, t)$ are represented by solid and dashed lines, respectively.

the internuclear region suggests the possibility of transient bond-weakening, in particular when there is significant population of these high-lying orbitals. These observations highlight the significant differences in the response of the H_2 molecule to a static magnetic field and a dynamic magnetic field.

The time-dependent magnetic fields considered here are extreme, chosen to match those studied previously using numerical grid-based calculations.^{47,51} Such fields provide a useful stress-test for our finite basis set implementation. It is therefore reassuring that the observations for H_2 under these exotic conditions are consistent with Ref. 51, suggesting that the approach implemented in the present work should be reliable for a wide range of applied fields, even in relatively modest basis sets.

2. Magnetic field orientation

In Secs. III A and III B 1, we have established the reliability of the finite basis set approach relative to available numerical grid-based methods for systems under extreme time-dependent magnetic fields. However, such benchmark studies tend to be limited to systems with specific symmetries, in particular, either spherical atoms or diatomic molecular systems in which the magnetic-field direction is coincident with the internuclear axis, where cylindrical symmetry can then be exploited. Furthermore, for these cases, the gauge-origin can be chosen such that LAOs are not required. It is therefore interesting to consider how the response of the H_2 molecule varies with respect to orientation relative to the applied time-dependent magnetic field. At non-parallel orientations, the orbitals are unavoidably complex, and this provides a more challenging test for the propagation of the electronic structure as the complex phase factors change rapidly with the oscillating magnetic field. Preliminary studies showed that in these orientations it was necessary

to reduce the time step significantly to achieve stable dynamics, and in particular, $\Delta t = 0.025$ a.u. was employed in these calculations (similar results were obtained with $\Delta t_S = 0.035$ a.u.).

Changes in orientation also alter the symmetry of the system significantly. The $D_{\infty h}$ symmetry in the absence of a field is reduced to $C_{\infty h}$ symmetry in a parallel field. For other non-parallel orientations, the symmetry is further reduced to C_i with the exception of the perpendicular orientation, which has C_{2h} symmetry. The molecular orbitals in the C_i and C_{2h} point groups are classified as *gerade* (*g*) or *ungerade* (*u*), and just as was observed for the parallel orientation, only $g \leftrightarrow g$ transitions are allowed according to the magnetic-dipole selection rules. As a result, all of the molecular orbitals with significant population during the dynamics have A_g symmetry. The projected orbital occupations of Eq. (16) show whether the orbitals in the presence of the field have σ , π , or δ character. In many cases, the high field A_g orbitals have a mixed character and the correspondence between the zero-field and high field orbitals has again been mapped out using the maximum-overlap method for each orientation.

To investigate the orientation effects, we considered time-dependent fields with $|\mathbf{B}_{\max}| = 0.8B_0$ and incident frequency $\omega = 0.767$ a.u. at a range of orientations between 10° and 90° relative to the internuclear axis. In Fig. 9, we show the projected occupation numbers for 30° , 60° , and 90° ; other orientations are presented in the supplementary material. Initially, the variation of the occupation numbers remains similar to that observed in Fig. 6 with similar orbitals contributing at angles up to 25° ; see Figs. S2, S4, S6, and S8. In particular, the projected occupation numbers suggest orbital contributions with mainly σ_g^+ character with some minor contributions of π_g character appearing for angles of 20° – 25° . The molecular orbitals corresponding to those identified by the zero-field projec-

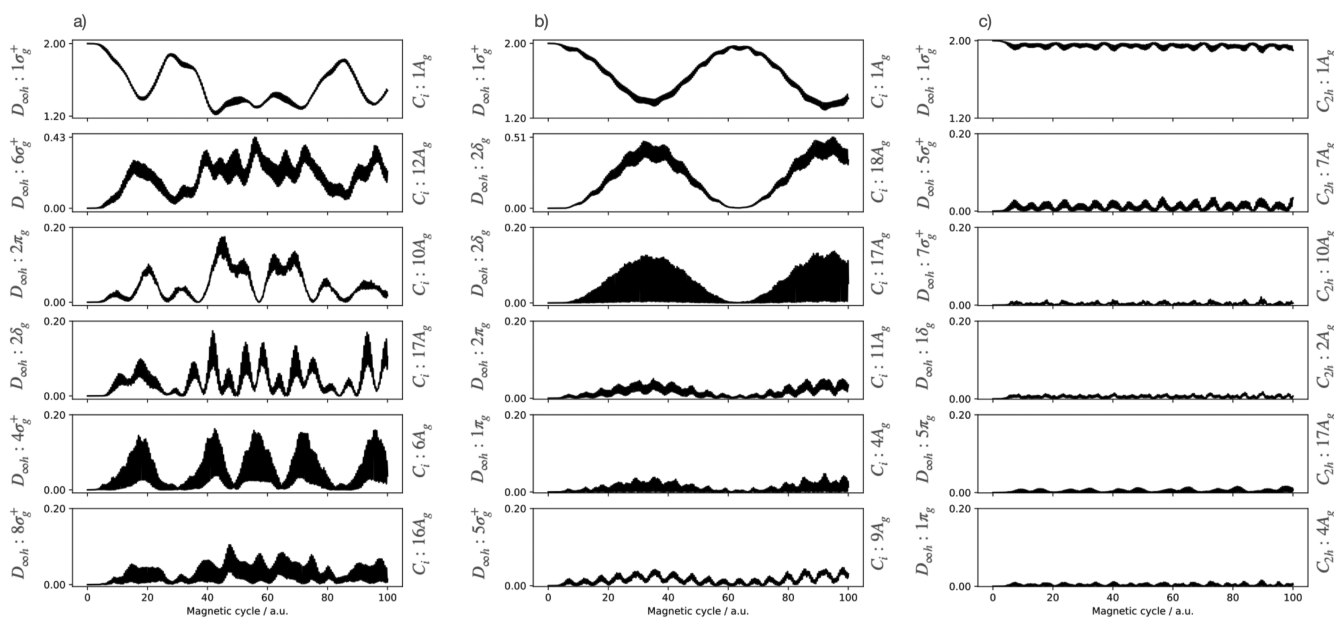


FIG. 9. The orbital populations of the H_2 molecule in a time-dependent magnetic field with $|\mathbf{B}_{\max}| = 0.8B_0$ oriented at (a) 30° , (b) 60° , and (c) 90° relative to the internuclear axis, computed at the RT-TDHF/aug-cc-pVTZ level. Note that the same value of the incident frequency of the time-dependent magnetic field $\omega = 0.767$ a.u. is used.

tions were also calculated using the maximum-overlap method for the same orientations with $|\mathbf{B}| = 0.8B_0$ and are presented in Figs. S3, S5, S7, and S9. The complex nature of the orbitals in the presence of a non-parallel magnetic field is clear from the colors of the iso-surfaces in each inset. It is also clear that the orbitals re-align as the orientation of the field changes (all iso-surfaces are presented viewed directly along the y axis).

At orientations in the range 25° – 35° , the observed dynamics changes dramatically. This is shown in the projected occupation number variation in Fig. 9(a), compared with Fig. 6. The projected occupations reveal that the A_g orbitals occupied during the dynamics have significant π and δ character at this orientation. In particular, there is significant character from the $2\pi_g$ and $2\delta_g$ orbitals. The relevant orbitals and the corresponding orbitals in the presence of a field are shown in Fig. 10. Again, the complex nature of the orbitals is clearly visible in the inset iso-surfaces with continuous colors indicating a wide range of complex phase angles. The oblique alignment of some of the molecular orbitals also leads to apparent distortions in the contour plots of the square modulus of the orbitals in the xz -plane. It is clear that the orientation of the magnetic field has a very significant influence on which orbitals are populated in the dynamics and that the involvement of orbitals with π and δ character leads to more prolonged periods where the lowest orbital is

depopulated. Since at these orientations, the molecular point group is C_i , several orbitals with A_g symmetry have suitable symmetry and energies to be involved in the dynamics, significantly altering the long timescale dynamics observed for parallel orientations.

At an orientation of 40° , there is another dramatic change in the observed dynamics. At this orientation, most of the dynamics is quenched with only minor contributions from a higher-lying orbital with predominantly σ character (see Fig. S14). For orientations in the range 60° – 80° , significant long timescale dynamics is again observed; see, for example, Fig. 9(b), where at 60° two A_g orbitals with δ -character are significantly involved in the dynamics. At these orientations, the π character orbitals play a much less significant role and the overall long timescale dynamics is simpler as a result with population oscillating between the lowest orbital and two A_g orbitals with δ -character. The orbitals involved in these transitions are shown in Fig. 11.

As the angle of the magnetic field increases from 60° , the period of the long timescale dynamics increases. At angles approaching 90° , the dynamics is again quenched until in the perpendicular orientation little dynamics is observed with the electrons remaining essentially in the lowest molecular orbital throughout. In general, these observations show that orientation relative to the magnetic field plays a very significant role in nature of the observed dynam-

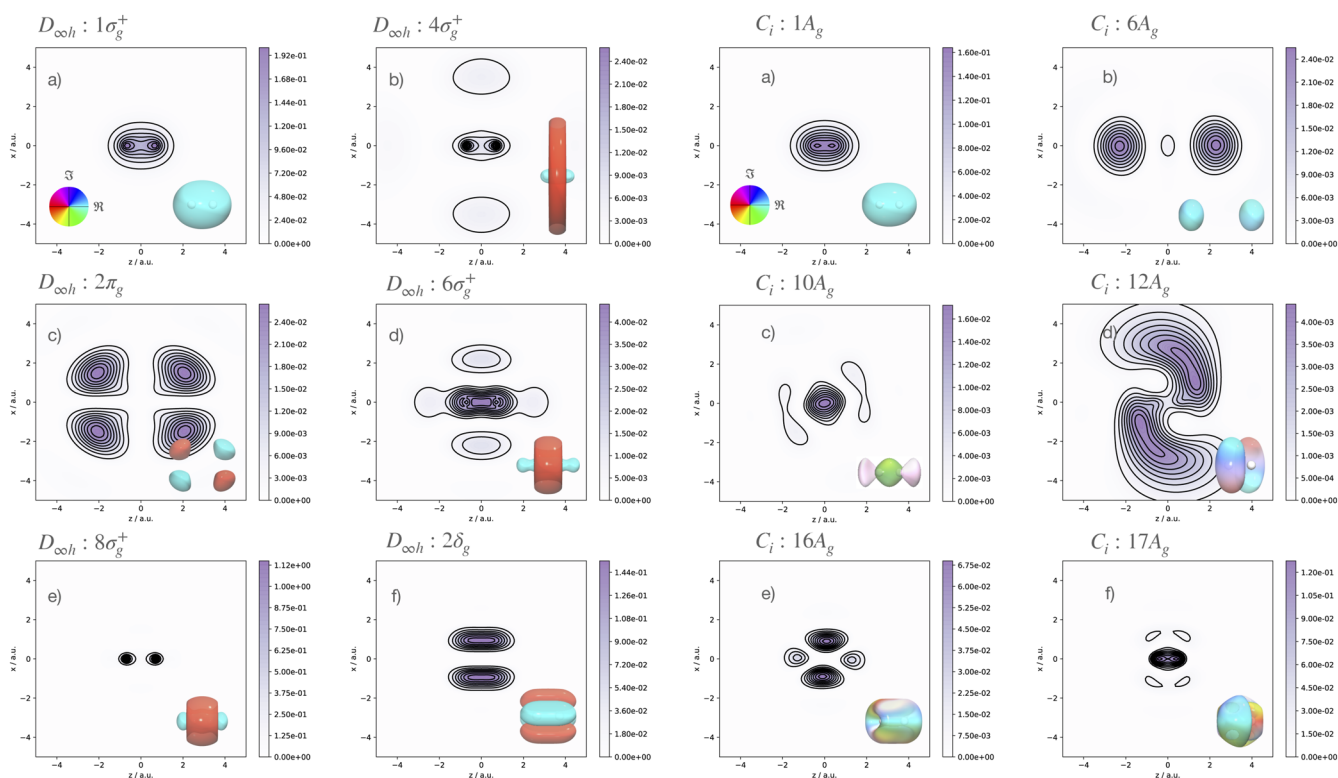


FIG. 10. The molecular orbitals that acquire significant population during the dynamics of the H_2 molecule in a time-dependent magnetic field with $|\mathbf{B}_{\max}| = 0.8B_0$ oriented at 30° to the internuclear axis according to the populations of Eq. (16). The orbitals are computed at the HF/aug-cc-pVTZ level in the absence of an external magnetic field [left panels (a)–(f)] and in a static external magnetic field oriented at 30° with $|\mathbf{B}| = 0.8B_0$ [right panels (a)–(f)]. Iso-surfaces of each orbital are shown as insets, color-coded according to the color wheel shown in panels (a). In the absence of a magnetic field, the point group is $D_{\infty h}$, which is reduced to C_i in the field.

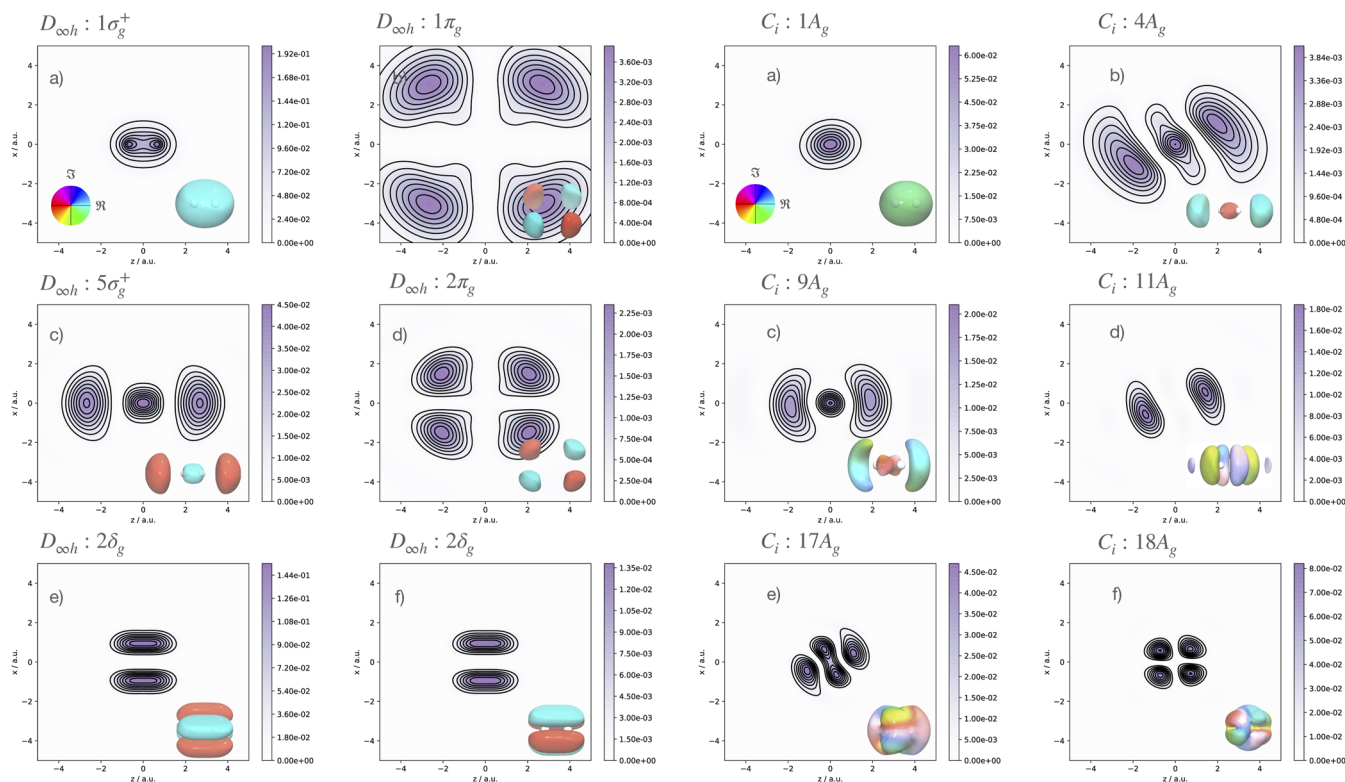


FIG. 11. The molecular orbitals that acquire significant population during the dynamics of the H_2 molecule in a time-dependent magnetic field with $|\mathbf{B}_{\text{max}}| = 0.8B_0$ oriented at 60° to the internuclear axis according to the populations of Eq. (16). The orbitals are computed at the HF/aug-cc-pVTZ level in the absence of an external magnetic field [left panels (a)–(f)] and in a static external magnetic field oriented at 60° with $|\mathbf{B}| = 0.8B_0$ [right panels (a)–(f)]. Iso-surfaces of each orbital are shown as insets, color-coded according to the color wheel shown in panels (a). In the absence of a magnetic field, the point group is $D_{\infty h}$, which is reduced to C_i in the field.

ics. The precise nature of the long-term dynamics correlates with the σ , π , δ , or mixed character of the orbitals involved. When mixed transitions are involved, very complex dynamics can be observed as was shown for orientations between 25° and 35° , whereas when only δ -character orbitals are involved as in the range 60° – 80° , simpler long timescale dynamics are observed. The results highlight the need to consider molecular orientation carefully in tandem with electron dynamics in such strong, rapidly varying fields. Indeed, a full consideration of nuclear motion and dynamics may be necessary.

IV. CONCLUSIONS

An implementation of real-time self-consistent field electronic structure methods with dynamical time-dependent magnetic fields has been presented using finite atomic orbital basis sets. Comparisons against benchmark numerical studies from the literature on the hydrogen atom and the H_2 molecule aligned parallel to the magnetic field have demonstrated the validity of the approach even for relatively extreme rapidly oscillating strong magnetic fields. Interestingly, the basis set requirements for the description of coherent emission, analogous to high-harmonic generation in intense electric fields, are relatively benign. Some care is required to ensure that sufficiently high angular momentum functions are included,

but otherwise, relatively compact standard basis sets are sufficient. The electron dynamics in the H_2 molecule under a strong parallel magnetic field were considered in detail, and fluctuations indicating transient bond strengthening and weakening were observed, consistent with previous studies and further confirming the applicability of the approach to molecular systems.

The finite basis set implementation uses London atomic orbitals and therefore allows for arbitrary orientation of the molecular frame relative to the applied field, overcoming a significant limitation of previous studies. The effect of orientation on the observed dynamics in the H_2 molecule in a strong time-dependent magnetic field was studied in detail. The use of unitary symmetry analysis including the magnetic field gave insight into the orbitals involved, and projection of the orbital occupations onto the initial orbitals in the absence of a magnetic field give insight into the σ , π , and δ characters of the orbitals in the reduced symmetries associated with different orientations of the applied magnetic field. It was observed that orientation has a profound effect on the observed dynamics with significant changes in both the timescale of the dynamics and the nature of the orbitals involved in the underlying transitions. Longer timescale dynamics was observed when the orbitals involved had significant π or δ character. Overall, the results suggest that it may be imperative to include orientation effects in the

study of systems under strong fields and perhaps highly desirable to include a more comprehensive treatment of nuclear dynamics. We note that recent studies have made significant progress in treating nuclear dynamics under static uniform external magnetic fields^{59–63} and this may be an interesting avenue for future study.

The framework introduced in the present work is rather flexible and already allows for the simultaneous application of time-dependent electric and magnetic fields. A key observation is that a time-dependent magnetic field allows for the study of magnetic-dipole allowed transitions, which would be otherwise inaccessible to standard RT-TDSCF implementations with time-dependent electric fields. In the present work, extreme rapidly oscillating magnetic fields were considered to stress-test the finite basis set implementation against benchmark numerical results for small systems. However, magnetic-dipole allowed transitions are of significance to EPR and NMR spectroscopies, and future work will examine how the tools developed here for time-dependent magnetic fields can be applied to these areas.

SUPPLEMENTARY MATERIAL

The supplementary material presents the additional information of the electron density of the H₂ molecule in a parallel time-dependent magnetic field, the 1σ_g and higher-lying orbital populations, and the molecular orbitals that acquire significant population during the dynamics of the H₂ molecule in different orientations of the time-dependent magnetic field.

ACKNOWLEDGMENTS

We acknowledge financial support from the European Research Council under the European Union's H2020 research and innovation program/ERC Consolidator Grant topDFT (Grant Agreement No. 772259). This work was supported by the Norwegian Research Council through the CoE Hylleraas Centre for Quantum Molecular Sciences Grant No. 262695. The authors are grateful to Dr. B. C. Huynh and Dr. T. J. P. Irons for useful discussions.

AUTHOR DECLARATIONS

Conflict of Interest

The authors have no conflicts to disclose.

Author Contributions

Meilani Wibowo-Teale: Conceptualization (equal); Formal analysis (equal); Investigation (equal); Methodology (equal); Writing – original draft (equal); Writing – review & editing (equal). **Benjamin J. Ennifer:** Formal analysis (equal); Investigation (equal); Methodology (equal); Writing – original draft (equal); Writing – review & editing (equal). **Andrew M. Wibowo-Teale:** Conceptualization (equal); Formal analysis (equal); Funding acquisition (lead); Investigation (equal); Methodology (equal); Writing – original draft (equal); Writing – review & editing (equal).

DATA AVAILABILITY

The data that support the findings of this study are available within the article and its supplementary material.

REFERENCES

- 1 M. D. Jones, G. Ortiz, and D. M. Ceperley, *Phys. Rev. A* **54**, 219 (1996).
- 2 S. Jordan, P. Schmelcher, W. Becken, and W. Schweizer, *Astron. Astrophys.* **336**, L33 (1998).
- 3 M. D. Jones, G. Ortiz, and D. M. Ceperley, *Phys. Rev. A* **59**, 2875 (1999).
- 4 M. V. Ivanov and P. Schmelcher, *Phys. Rev. A* **60**, 3558 (1999).
- 5 P. Schmelcher and L. S. Cederbaum, *Phys. Rev. A* **37**, 672 (1988).
- 6 D. Wickramasinghe and L. Ferrario, *Publ. Astron. Soc. Pac.* **112**, 873 (2000).
- 7 Z. Medin and D. Lai, *Phys. Rev. A* **74**, 062507 (2006).
- 8 W. Becken, P. Schmelcher, and F. K. Diakonou, *J. Phys. B: At., Mol. Opt. Phys.* **32**, 1557 (1999).
- 9 W. Becken and P. Schmelcher, *Phys. Rev. A* **63**, 053412 (2001).
- 10 W. Becken and P. Schmelcher, *Phys. Rev. A* **65**, 033416 (2002).
- 11 G. Ortiz, M. D. Jones, and D. M. Ceperley, *Phys. Rev. A* **52**, R3405 (1995).
- 12 M. D. Jones, G. Ortiz, and D. M. Ceperley, *Int. J. Quantum Chem.* **64**, 523 (1997).
- 13 M. D. Jones, G. Ortiz, and D. M. Ceperley, *Phys. Rev. E* **55**, 6202 (1997).
- 14 K. K. Lange, E. I. Tellgren, M. R. Hoffmann, and T. Helgaker, *Science* **337**, 327 (2012).
- 15 E. I. Tellgren, A. Soncini, and T. Helgaker, *J. Chem. Phys.* **129**, 154114 (2008).
- 16 E. I. Tellgren, T. Helgaker, and A. Soncini, *Phys. Chem. Chem. Phys.* **11**, 5489 (2009).
- 17 E. I. Tellgren, S. S. Reine, and T. Helgaker, *Phys. Chem. Chem. Phys.* **14**, 9492 (2012).
- 18 E. I. Tellgren and H. Fliegl, *J. Chem. Phys.* **139**, 164118 (2013).
- 19 E. I. Tellgren, A. M. Teale, J. W. Furness, K. K. Lange, U. Ekström, and T. Helgaker, *J. Chem. Phys.* **140**, 034101 (2014).
- 20 S. Stopkowicz, J. Gauss, K. K. Lange, E. I. Tellgren, and T. Helgaker, *J. Chem. Phys.* **143**, 074110 (2015).
- 21 F. Hampe and S. Stopkowicz, *J. Chem. Phys.* **146**, 154105 (2017).
- 22 F. Hampe and S. Stopkowicz, *J. Chem. Theory Comput.* **15**, 4036 (2019).
- 23 S. Sen, K. K. Lange, and E. I. Tellgren, *J. Chem. Theory Comput.* **15**, 3974 (2019).
- 24 J. Austad, A. Borgoo, E. I. Tellgren, and T. Helgaker, *Phys. Chem. Chem. Phys.* **22**, 23502 (2020).
- 25 J. W. Furness, J. Verbeke, E. I. Tellgren, S. Stopkowicz, U. Ekström, T. Helgaker, and A. M. Teale, *J. Chem. Theory Comput.* **11**, 4169 (2015).
- 26 T. J. P. Irons, J. Zemen, and A. M. Teale, *J. Chem. Theory Comput.* **13**, 3636 (2017).
- 27 T. J. P. Irons, L. Spence, G. David, B. T. Speake, T. Helgaker, and A. M. Teale, *J. Phys. Chem. A* **124**, 1321 (2020).
- 28 A. Pausch and W. Klopper, *Mol. Phys.* **118**, e1736675 (2020).
- 29 T. J. P. Irons, G. David, and A. M. Teale, *J. Chem. Theory Comput.* **17**, 2166 (2021).
- 30 S. Reimann, A. Borgoo, J. Austad, E. I. Tellgren, A. M. Teale, T. Helgaker, and S. Stopkowicz, *Mol. Phys.* **117**, 97 (2018).
- 31 M. Wibowo, T. J. P. Irons, and A. M. Teale, *J. Chem. Theory Comput.* **17**, 2137 (2021).
- 32 G. David, T. J. P. Irons, A. E. A. Fouda, J. W. Furness, and A. M. Teale, *J. Chem. Theory Comput.* **17**, 5492 (2021).
- 33 A. Pausch, M. Gebele, and W. Klopper, *J. Chem. Phys.* **155**, 201101 (2021).
- 34 M. J. Pemberton, T. J. P. Irons, T. Helgaker, and A. M. Teale, *J. Chem. Phys.* **156**, 204113 (2022).
- 35 R. Francotte, T. J. P. Irons, A. M. Teale, F. de Proft, and P. Geerlings, *Chem. Sci.* **13**, 5311 (2022).
- 36 T. J. P. Irons, B. C. Huynh, A. M. Teale, F. de Proft, and P. Geerlings, *Mol. Phys.* (published online 2022).

- ³⁷M. Wibowo, B. C. Huynh, C. Y. Cheng, T. J. P. Irons, and A. M. Teale, *Mol. Phys.* **121**, e2152748 (2022).
- ³⁸G. D. Schmidt, R. G. Allen, P. S. Smith, and J. Liebert, *Astrophys. J.* **463**, 320 (1996).
- ³⁹C. Vikas, *Chem. Phys. Lett.* **413**, 216 (2005).
- ⁴⁰M. Sadhukhan, P. K. Panigrahi, and B. M. Deb, *Europhys. Lett.* **91**, 23001 (2010).
- ⁴¹Vikas, *Eur. Phys. J. D* **66**, 5 (2012).
- ⁴²N. Goel, S. Gupta, M. Sadhukhan, and B. M. Deb, *Mol. Phys.* **118**, e1676930 (2019).
- ⁴³E. Coccia, B. Mussard, M. Labeye, J. Caillat, R. Taïeb, J. Toulouse, and E. Luppi, *Int. J. Quantum Chem.* **116**, 1120 (2016).
- ⁴⁴F. London, *J. Phys. Radium* **8**, 397 (1937).
- ⁴⁵J. Almlöf, K. Fægri, and K. Korsell, *J. Comput. Chem.* **3**, 385 (1982).
- ⁴⁶QUEST, A rapid development platform for quantum electronic structure techniques, <https://quest.codes>, 2019.
- ⁴⁷M. Sadhukhan and B. Deb, *J. Mol. Struct.: THEOCHEM* **943**, 65 (2010).
- ⁴⁸M. Sadhukhan and B. M. Deb, *Phys. Rev. A* **89**, 042516 (2014).
- ⁴⁹F. Plasser, M. Ruckebauer, S. Mai, M. Oppel, P. Marquetand, and L. González, *J. Chem. Theory Comput.* **12**, 1207 (2016).
- ⁵⁰J. H. Shirley, *Phys. Rev.* **138**, B979 (1965).
- ⁵¹M. Sadhukhan and B. M. Deb, *Mol. Phys.* **114**, 3490 (2016).
- ⁵²A. J. Ceulemans, *Group Theory Applied to Chemistry* (Springer, Dordrecht, 2013).
- ⁵³R. R. Birss, *Symmetry and Magnetism* (North-Holland Publishing Co., Amsterdam, 1966).
- ⁵⁴P. Lazzeretti, M. Malagoli, and R. Zanasi, "NATO ASI series: Electronic current density induced by magnetic fields and magnetic moments in molecules," in *Nuclear Magnetic Shieldings and Molecular Structure*, edited by J. A. Tossell (Springer Science + Business Media, B.V., Maryland, 1993), p. 163.
- ⁵⁵S. Pelloni and P. Lazzeretti, *Int. J. Quantum Chem.* **111**, 356 (2011).
- ⁵⁶C. J. Bradley and B. L. Davies, *Rev. Mod. Phys.* **40**, 359 (1968).
- ⁵⁷E. Wigner, *Group Theory and its Application to the Quantum Mechanics of Atomic Spectra* (Academic Press, London, 1959).
- ⁵⁸A. P. Cracknell, *Prog. Theor. Phys.* **35**, 196 (1966).
- ⁵⁹T. Culpitt, L. D. M. Peters, E. I. Tellgren, and T. Helgaker, *J. Chem. Phys.* **155**, 024104 (2021).
- ⁶⁰L. D. M. Peters, T. Culpitt, L. Monzel, E. I. Tellgren, and T. Helgaker, *J. Chem. Phys.* **155**, 024105 (2021).
- ⁶¹T. Culpitt, L. D. M. Peters, E. I. Tellgren, and T. Helgaker, *J. Chem. Phys.* **156**, 044121 (2022).
- ⁶²L. Monzel, A. Pausch, L. D. M. Peters, E. I. Tellgren, T. Helgaker, and W. Klopper, *J. Chem. Phys.* **157**, 054106 (2022).
- ⁶³L. D. M. Peters, T. Culpitt, E. I. Tellgren, and T. Helgaker, *J. Chem. Phys.* **157**, 134108 (2022).